

NASA/TM-2017-219667



# Comparison of Theodorsen's Unsteady Aerodynamic Forces with Doublet Lattice Generalized Aerodynamic Forces

*Boyd Perry, III*  
*Langley Research Center, Hampton, Virginia*

## NASA STI Program . . . in Profile

Since its founding, NASA has been dedicated to the advancement of aeronautics and space science. The NASA scientific and technical information (STI) program plays a key part in helping NASA maintain this important role.

The NASA STI program operates under the auspices of the Agency Chief Information Officer. It collects, organizes, provides for archiving, and disseminates NASA's STI. The NASA STI program provides access to the NTRS Registered and its public interface, the NASA Technical Reports Server, thus providing one of the largest collections of aeronautical and space science STI in the world. Results are published in both non-NASA channels and by NASA in the NASA STI Report Series, which includes the following report types:

- **TECHNICAL PUBLICATION.** Reports of completed research or a major significant phase of research that present the results of NASA Programs and include extensive data or theoretical analysis. Includes compilations of significant scientific and technical data and information deemed to be of continuing reference value. NASA counter-part of peer-reviewed formal professional papers but has less stringent limitations on manuscript length and extent of graphic presentations.
- **TECHNICAL MEMORANDUM.** Scientific and technical findings that are preliminary or of specialized interest, e.g., quick release reports, working papers, and bibliographies that contain minimal annotation. Does not contain extensive analysis.
- **CONTRACTOR REPORT.** Scientific and technical findings by NASA-sponsored contractors and grantees.

- **CONFERENCE PUBLICATION.** Collected papers from scientific and technical conferences, symposia, seminars, or other meetings sponsored or co-sponsored by NASA.
- **SPECIAL PUBLICATION.** Scientific, technical, or historical information from NASA programs, projects, and missions, often concerned with subjects having substantial public interest.
- **TECHNICAL TRANSLATION.** English-language translations of foreign scientific and technical material pertinent to NASA's mission.

Specialized services also include organizing and publishing research results, distributing specialized research announcements and feeds, providing information desk and personal search support, and enabling data exchange services.

For more information about the NASA STI program, see the following:

- Access the NASA STI program home page at <http://www.sti.nasa.gov>
- E-mail your question to [help@sti.nasa.gov](mailto:help@sti.nasa.gov)
- Phone the NASA STI Information Desk at 757-864-9658
- Write to:  
NASA STI Information Desk  
Mail Stop 148  
NASA Langley Research Center  
Hampton, VA 23681-2199

NASA/TM-2017-219667



# Comparison of Theodorsen's Unsteady Aerodynamic Forces with Doublet Lattice Generalized Aerodynamic Forces

*Boyd Perry, III*  
*Langley Research Center, Hampton, Virginia*

National Aeronautics and  
Space Administration

Langley Research Center  
Hampton, Virginia 23681-2199

---

September 2017

# Errata

Issued October 24, 2017 for

NASA-TM-2017-219667

Comparison of Theodorsen's Unsteady Aerodynamic Forces  
with Doublet Lattice Generalized Aerodynamic Forces

by

Boyd Perry, III

*Summary of Changes:*

*Table 1 (p. 16) and Table 3 (p. 17) have incorrect row and column headings.  
The row headings should be "i=\_ " and the column headings should be "j=\_ ".*

*Corrected Table 1 –*

<b>Percentage Differences Between Complex Absolute Values at <math>k = 0.5</math></b>			
	<b><math>j = 1</math></b>	<b><math>j = 2</math></b>	<b><math>j = 3</math></b>
<b><math>i = 1</math></b>	0.57	0.88	1.16
<b><math>i = 2</math></b>	0.57	1.91	0.70
<b><math>i = 3</math></b>	2.56	6.76	0.87

*Corrected Table 3 –*

<b>Procrustes Distances for -</b>			
	<b><math>j = 1</math></b>	<b><math>j = 2</math></b>	<b><math>j = 3</math></b>
<b><math>i = 1</math></b>	0.0455	0.0625	0.0242
<b><math>i = 2</math></b>	0.0394	0.0527	0.0086
<b><math>i = 3</math></b>	0.1544	0.2813	0.0191

### **Acknowledgments**

The author wishes to acknowledge the valuable contributions to this paper made by Ms. Carol D. Wieseman of the NASA Langley, Aeroelasticity Branch and Mr. G. Lee Pollard of NCI Information Systems, Inc. Ms. Wieseman performed all of the Doublet Lattice calculations reported in this paper. Mr. Pollard produced all the final figures in this paper. Many thanks to you both!

The use of trademarks or names of manufacturers in this report is for accurate reporting and does not constitute an official endorsement, either expressed or implied, of such products or manufacturers by the National Aeronautics and Space Administration.

Available from:

NASA STI Program / Mail Stop 148  
NASA Langley Research Center  
Hampton, VA 23681-2199  
Fax: 757-864-6500

## **Abstract**

*This paper identifies the unsteady aerodynamic forces and moments for a typical section contained in the NACA Report No. 496, "General Theory of Aerodynamic Instability and the Mechanism of Flutter," by Theodore Theodorsen. These quantities are named Theodorsen's aerodynamic forces (TAFs). The TAFs are compared to the generalized aerodynamic forces (GAFs) for a very high aspect ratio wing ( $AR = 20$ ) at zero Mach number computed by the doublet lattice method. Agreement between TAFs and GAFs is very-good-to-excellent. The paper also reveals that simple proportionality relationships that are known to exist between the real parts of some GAFs and the imaginary parts of others also hold for the real and imaginary parts of the corresponding TAFs.*

THIS PAGE INTENTIONALLY LEFT BLANK

## I. INTRODUCTION

Reference 1 by the present author contains the recomputation of all numerical examples in reference 2, the seminal and ground-breaking work on aeroelastic flutter by Theodore Theodorsen. While performing these recomputations, the present author explored a number of related “tangents.” One such tangent was to investigate the similarity between the unsteady aerodynamic forces and moments derived in reference 2 (termed herein “Theodorsen’s aerodynamic forces,” or TAFs) and the generalized aerodynamic forces (GAFs) of the doublet lattice method (DLM) (ref. 3).

The purpose of the present paper is to report the results of this tangential investigation. Analytical expressions for the TAFs were extracted from Theodorsen’s aeroelastic equations of motion (AEOM) for a typical airfoil section (referred to hereinafter simply as “typical section”) in incompressible flow and are compared to the GAFs computed by the DLM for a high-aspect-ratio wing ( $AR = 20$ ) at zero Mach number. Simple proportionality relationships that are known to exist between the real parts of some GAFs and the imaginary parts of others are shown to hold for the real and imaginary parts of the corresponding TAFs.

The results of the present paper are more curiosity than revelation, and more interest than discovery. After all, Theodorsen’s AEOM and the DLM have both been around for a long time. But, in conducting a literature search, the present author could find no publication that contained comparisons similar to those contained herein. So, for this reason, it was judged that the present results are worth sharing with the technical community.

The remainder of this paper is organized as follows:

Section II presents nomenclature;

Section III addresses the recasting of Theodorsen’s AEOM into the classical form of the AEOM so that the comparison of TAFs and GAFs may be accomplished;

Section IV presents analytical expressions for the TAFs;

Section V addresses the approximation of a typical section using the DLM;

Section VI presents the calculation of the TAFs and GAFs;

Section VII presents the comparison of the TAFs and GAFs;

Section VIII discusses relationships among the TAFs that are analogous to relationships among the GAFs;

Section IX contains concluding remarks;

Appendix A presents a brief examination of Theodorsen’s circulation function;

Appendix B presents the DLM aerodynamic model chosen to compute the GAFs.



## II. NOMENCLATURE

$a$	Nondimensional distance from midchord to axis of rotation (elastic axis) of typical section, positive aft
$b$	Semichord of typical section
$\bar{b}$	Mean aerodynamic semichord, $\frac{\bar{c}}{2}$
$C(k)$	Theodorsen's circulation function
$C_{L\alpha}$	Lift curve slope
$C_{m\alpha}$	Static stability derivative
$C_\alpha$	Torsional stiffness of typical section (stiffness units per unit length)
$C_\beta$	Aileron stiffness of typical section (stiffness units per unit length)
$C_h$	Bending stiffness of typical section (stiffness units per unit length)
$\Delta C_p(x)$	Incremental pressure coefficient due to pitch
$c$	Nondimensional distance from midchord to aileron hinge of typical section, positive aft
$\bar{c}$	Wing mean aerodynamic chord
$F(k)$	Real part of Theodorsen's circulation function
$G(k)$	Imaginary part of Theodorsen's circulation function
$h$	Plunge deflection, Classical AEOM, positive down
$h$	Vertical deflection, Theodorsen's AEOM, positive down
$\mathbb{I}$	Imaginary part, equation (7)
$i$	Imaginary unit, $\sqrt{-1}$
$J_i(k)$	Bessel function of the first kind, subscript $i$ denotes order
$k$	Reduced frequency, $\frac{\omega b}{v}$
$\mathbb{k}$	Constant, equation (7)
$M$	Mass of typical section (mass units per unit length)
$Q_{ijReal}$	Real part of $ij^{th}$ element of $Q$
$Q_{ijImag}$	Imaginary part of $ij^{th}$ element of $Q$
$\tilde{Q}_{ijReal}$	Real part of $ij^{th}$ element of $\tilde{Q}$
$\tilde{Q}_{ijImag}$	Imaginary part of $ij^{th}$ element of $\tilde{Q}$

$q$	Dynamic pressure, $\frac{1}{2}\rho v^2$
$\mathbb{R}$	Real part, equation (7)
$r_\alpha$	Nondimensional torsional radius of gyration of typical section
$r_\beta$	Nondimensional radius of gyration of aileron
$S$	Wing area
$T_i$	Constants associated with the integration of velocity potentials in reference 2, for $i = 1, 3, 4, 5, 7, 10, 11, 12$
$v$	Free-stream velocity
$x$	Chordwise coordinate, Figure 1, $-1 \leq x \leq 1$
$x_\alpha$	Nondimensional distance from axis of rotation to center of gravity, positive aft
$x_\beta$	Nondimensional distance from aileron hinge to aileron center of gravity, positive aft
$Y_i(k)$	Bessel function of the second kind, subscript $i$ denotes order
$\alpha$	Pitch deflection, Classical AEOM, positive leading edge up
$\alpha$	Torsional angular deflection, Theodorsen's AEOM, positive leading edge up
$\beta$	Aileron angular deflection, positive trailing edge down
$\kappa$	Mass ratio, $\frac{\pi\rho b^2}{M}$
$\rho$	Fluid density
$\omega$	Circular frequency
$\omega_h$	Circular frequency of flexure mode
$\omega_\alpha$	Circular frequency of torsional mode
$\omega_\beta$	Circular frequency of aileron mode
Matrices:	
$[\mathcal{A}]$	Matrix containing coefficients of acceleration terms in equations (A), (B), and (C)
$[\mathcal{B}]$	Matrix containing coefficients of rate terms in equations (A), (B), and (C)
$[\mathcal{C}]$	Matrix containing coefficients of displacement terms in equations (A), (B), and (C)
$[K]$	Generalized stiffness matrix
$[M]$	Generalized mass matrix
$[Q(k)]$	Theodorsen's aerodynamic force matrix

$[\tilde{Q}(k)]$	Generalized aerodynamic force matrix
$\{q\}$	Vector of generalized coordinates
$[Z]$	Generalized damping matrix

Abbreviations:

AEOM	Aeroelastic equations of motion
AR	Aspect ratio
DLM	Doublet lattice method
GAF	Generalized aerodynamic force
LE	Leading edge
OPA	Ordinary Procrustes Analysis
RMSD	Root mean square distance
SSD	Sum of the squared distances
TAF	Theodorsen's aerodynamic force
TE	Trailing edge

One or two dots over a quantity indicate, respectively, the first or second time derivative of that quantity.

### III. RECASTING THEODORSEN'S AEROELASTIC EQUATIONS OF MOTION

In order to directly compare TAFs and GAFs, Theodorsen's aeroelastic equations of motion (AEOM) must be recast into a more convenient form. This section of the present paper describes the recasting.

#### Theodorsen's Equations

Reference 2 derives from first principles the AEOM for a typical section with degrees of freedom in torsion ( $\alpha$ ), aileron deflection ( $\beta$ ), and vertical deflection (sometimes referred to as flexure) ( $h$ ). Figure 1 illustrates the definitions and positive senses of many of the important parameters appearing in Theodorsen's AEOM.

Assumptions inherent in Theodorsen's development of the equations are (1) the flow is potential and non-stationary; (2) the "wing" is actually a two-dimensional typical section with no thickness and therefore with no airfoil shape; (3) the wing motions are sinusoidal and infinitesimal; and (4) the wing has no internal or solid friction, resulting in no internal damping forces. As a consequence of these assumptions, the resulting AEOM are very concise, and, by today's standards, are very simple, yet they retain the essential physical attributes of aeroelastic flutter.

Theodorsen's AEOM are three second-order simultaneous differential equations in the three unknowns,  $\alpha$ ,  $\beta$ , and  $h$ , and their first and second time derivatives, representing the sum of the moments about the elastic axis, the sum of the moments about the aileron hinge, and the sum of the forces on the entire wing in the vertical direction. Equations (A), (B), and (C), below, are reproduced from reference 2:

$$\begin{aligned}
\text{(A)} \quad & \ddot{\alpha} \left[ r_\alpha^2 + \kappa \left( \frac{1}{8} + a^2 \right) \right] + \dot{\alpha} \frac{v}{b} \kappa \left( \frac{1}{2} - a \right) + \alpha \frac{C_\alpha}{Mb^2} + \ddot{\beta} \left[ r_\beta^2 + (c-a)x_\beta - \frac{T_7}{\pi} \kappa - (c-a) \frac{T_1}{\pi} \kappa \right] + \frac{1}{\pi} \dot{\beta} \kappa \frac{v}{b} \left[ -2p - \left( \frac{1}{2} - a \right) T_4 \right] \\
& + \beta \kappa \frac{v^2}{b^2} \frac{1}{\pi} (T_4 + T_{10}) + \ddot{h} \left( x_\alpha - a\kappa \right) \frac{1}{b} - 2\kappa \left( a + \frac{1}{2} \right) \frac{vC(k)}{b} \left[ \frac{v\alpha}{b} + \frac{\dot{h}}{b} + \left( \frac{1}{2} - a \right) \dot{\alpha} + \frac{T_{10}}{\pi} \frac{v}{b} \beta + \frac{T_{11}}{2\pi} \dot{\beta} \right] = 0 \\
\text{(B)} \quad & \ddot{\alpha} \left[ r_\beta^2 + (c-a)x_\beta - \kappa \frac{T_7}{\pi} - (c-a) \frac{T_1}{\pi} \kappa \right] + \dot{\alpha} \left( p - T_1 - \frac{1}{2} T_4 \right) \frac{v}{b} \frac{\kappa}{\pi} + \ddot{\beta} \left( r_\beta^2 - \frac{1}{\pi} \kappa T_3 \right) - \frac{1}{2\pi^2} \dot{\beta} T_4 T_{11} \frac{v}{b} \kappa \\
& + \beta \left[ \frac{C_\beta}{Mb^2} + \frac{1}{\pi^2} \frac{v^2}{b^2} \kappa (T_5 - T_4 T_{10}) \right] + \ddot{h} \left( x_\beta - \frac{1}{\pi} \kappa T_1 \right) \frac{1}{b} + \frac{T_{12}}{\pi} \kappa \frac{vC(k)}{b} \left[ \frac{v\alpha}{b} + \frac{\dot{h}}{b} + \left( \frac{1}{2} - a \right) \dot{\alpha} + \frac{T_{10}}{\pi} \frac{v}{b} \beta + \frac{T_{11}}{2\pi} \dot{\beta} \right] = 0 \\
\text{(C)} \quad & \ddot{\alpha} \left( x_\alpha - \kappa a \right) + \dot{\alpha} \frac{v}{b} \kappa + \ddot{\beta} \left( x_\beta - \frac{1}{\pi} T_1 \kappa \right) - \dot{\beta} \frac{v}{b} T_4 \kappa \frac{1}{\pi} + \ddot{h} (1 + \kappa) \frac{1}{b} + \dot{h} \frac{C_h}{M} \frac{1}{b} \\
& + 2\kappa \frac{vC(k)}{b} \left[ \frac{v\alpha}{b} + \frac{\dot{h}}{b} + \left( \frac{1}{2} - a \right) \dot{\alpha} + \frac{T_{10}}{\pi} \frac{v}{b} \beta + \frac{T_{11}}{2\pi} \dot{\beta} \right] = 0
\end{aligned}$$

Unsteady circulatory aerodynamics are present in the form of the Theodorsen circulation function,  $C(k)$ , a complex function of reduced frequency, with real part  $F(k)$  and imaginary part  $G(k)$ , expressed in terms of Bessel functions. Appendix A contains a brief examination of this function.

While the form of equations (A), (B), and (C) was suitable for Theodorsen's purposes, it poses an obstacle to the present purpose of comparing TAFs and GAFs. Recasting equations (A), (B), and (C) into a more convenient form will eliminate this obstacle. This more convenient form is described next.

### Classical Equations

For many years the AEOM have been written in the following form, termed herein the "classical form,"

$$[M]\{\ddot{q}\} + [Z]\{\dot{q}\} + [K]\{q\} + \frac{1}{2}\rho v^2 [Q(k)]\{q\} = 0. \quad (1a)$$

where  $M$  is the generalized mass matrix,  $Z$  is the generalized damping matrix,  $K$  is the generalized stiffness matrix, and  $Q$  is the matrix of generalized aerodynamic forces, which are functions of reduced frequency. Quantity  $q$  is the vector of generalized coordinates and  $\frac{1}{2}\rho v^2$  is dynamic pressure. Reference 4 is one of many references that contain AEOM expressed in the classical form.

Typically, the AEOM expressed in the classical form are derived from Lagrange's equations using a modal approach with orthogonal modes, including rigid-body modes, flexible modes, and control-surface modes. Also, the AEOM expressed in the classical form usually account for the third physical dimension in modeling a flight vehicle. The classical form often employs the doublet lattice method (DLM) for computing unsteady aerodynamic forces.

The classical form of the AEOM was chosen in this paper because it lends itself so well to the purpose of comparing Theodorsen's aerodynamic forces (TAFs) found in equations (A), (B), and (C) to generalized aerodynamic forces (GAFs) computed by the DLM.

Equation (1a) is an alternate equivalent expression for equations (A), (B), and (C), where the generalized coordinates are  $\{q\} = \begin{Bmatrix} \alpha \\ \beta \\ h \end{Bmatrix}$ . Equations (A), (B), and (C) will be recast into the form of Equation (1a).

## Recasting

Recasting Theodorsen's AEOM into the form of the classical AEOM is a three-step process.

**Step one.** – The first step in recasting Theodorsen's AEOM into the form of equation (1a) is to rewrite equations (A), (B), and (C) into the following matrix form

$$[\mathcal{A}]\{\ddot{q}\} + [\mathcal{B}]\{\dot{q}\} + [\mathcal{C}]\{q\} = 0, \quad \text{where, again, } \{q\} = \begin{Bmatrix} \alpha \\ \beta \\ h \end{Bmatrix}. \quad (2a)$$

In equation (2a), the various terms in equations (A), (B), and (C) have been grouped into matrices according to vector  $q$  and its time derivatives:

$$\mathcal{A} = \begin{bmatrix} r_\alpha^2 + \kappa\left(\frac{1}{8} + a^2\right) & r_\beta^2 + (c - a)x_\beta - \kappa(c - a)\frac{T_1}{\pi} - \kappa\frac{T_7}{\pi} & \frac{x_\alpha}{b} - \kappa\frac{a}{b} \\ r_\beta^2 + (c - a)x_\beta - \kappa(c - a)\frac{T_1}{\pi} - \kappa\frac{T_7}{\pi} & r_\beta^2 - \kappa\frac{T_3}{\pi^2} & \frac{x_\beta}{b} - \kappa\frac{T_1}{\pi b} \\ x_\alpha - \kappa a & x_\beta - \kappa\frac{T_1}{\pi} & \frac{1}{b} + \kappa\frac{1}{b} \end{bmatrix}; \quad (3a)$$

$$\mathcal{B} = \kappa\frac{v}{b} \begin{bmatrix} \left(\frac{1}{2} - a\right) + C(k)2\left(a^2 - \frac{1}{4}\right) & \frac{1}{\pi}\left(-2p - \left(\frac{1}{2} - a\right)T_4\right) - C(k)\frac{1}{\pi}\left(a + \frac{1}{2}\right)T_{11} & -C(k)2\frac{1}{b}\left(a + \frac{1}{2}\right) \\ \frac{1}{\pi}\left(p - T_1 - \frac{T_4}{2}\right) + C(k)\frac{1}{\pi}\left(\frac{1}{2} - a\right)T_{12} & -\frac{1}{2\pi^2}T_4T_{11} + C(k)\frac{1}{2\pi^2}T_{11}T_{12} & C(k)\frac{1}{b\pi}T_{12} \\ 1 + C(k)2\left(\frac{1}{2} - a\right) & -\frac{1}{\pi}T_4 + C(k)\frac{1}{\pi}T_{11} & C(k)2\frac{1}{b} \end{bmatrix}; \quad (4a)$$

$$\mathcal{C} = \begin{bmatrix} \omega_a^2 r_\alpha^2 - \kappa\left(\frac{v}{b}\right)^2 C(k)2\left(a + \frac{1}{2}\right) & \kappa\left(\frac{v}{b}\right)^2 \frac{1}{\pi}(T_4 + T_{10}) - \kappa\left(\frac{v}{b}\right)^2 C(k)2\frac{1}{\pi}\left(a + \frac{1}{2}\right)T_{10} & 0 \\ \kappa\left(\frac{v}{b}\right)^2 C(k)\frac{1}{\pi}T_{12} & \omega_\beta^2 r_\beta^2 + \kappa\left(\frac{v}{b}\right)^2 \frac{1}{\pi^2}(T_5 - T_4T_{10}) + \kappa\left(\frac{v}{b}\right)^2 C(k)\frac{1}{\pi^2}T_{10}T_{12} & 0 \\ \kappa\left(\frac{v}{b}\right)^2 C(k)2 & \kappa\left(\frac{v}{b}\right)^2 C(k)2\frac{1}{\pi}T_{10} & \frac{\omega_h^2}{b} \end{bmatrix}. \quad (5a)$$

Matrices  $\mathcal{A}$ ,  $\mathcal{B}$ , and  $\mathcal{C}$  in equations (3a), (4a), and (5a) each contain structural terms and aerodynamic terms.

**Step two.** – The second step in recasting is to separate matrices  $\mathcal{A}$ ,  $\mathcal{B}$ , and  $\mathcal{C}$  into their constituent structural and aerodynamic parts. The structural parts may be further separated into mass and inertia terms, damping terms, and stiffness terms; the aerodynamic parts may be further separated into noncirculatory terms and circulatory terms (those containing  $C(k)$ ). The matrix subscripts “struct,” “non,” and “circ,” will be used to denote the structural parts, noncirculatory aerodynamic parts, and circulatory aerodynamic parts, respectively, of matrices  $\mathcal{A}$ ,  $\mathcal{B}$ , and  $\mathcal{C}$ . These constituent matrices are found in equations (3b) through (3d), equations (4b) through (4d), and equations (5b) through (5d), presented next.

The structural parts of matrices  $\mathcal{A}$ ,  $\mathcal{B}$ , and  $\mathcal{C}$  in equation (2a) are

$$\mathcal{A}_{struct} = \begin{bmatrix} r_\alpha^2 & r_\beta^2 + (c-a)x_\beta & x_\alpha/b \\ r_\beta^2 + (c-a)x_\beta & r_\beta^2 & x_\beta/b \\ x_\alpha & x_\beta & 1/b \end{bmatrix}, \quad (3b)$$

$$\mathcal{B}_{struct} = \begin{bmatrix} 0 & 0 & 0 \\ 0 & 0 & 0 \\ 0 & 0 & 0 \end{bmatrix}, \quad (4b)$$

(As stated above, Theodorsen did not include any structural damping terms in the derivation of his AEOM.)

$$\mathcal{C}_{struct} = \begin{bmatrix} \omega_\alpha^2 r_\alpha^2 & 0 & 0 \\ 0 & \omega_\beta^2 r_\beta^2 & 0 \\ 0 & 0 & \frac{\omega_h^2}{b} \end{bmatrix}. \quad (5b)$$

Matrices  $\mathcal{A}_{struct}$ ,  $\mathcal{B}_{struct}$ , and  $\mathcal{C}_{struct}$  correspond, respectively, to matrices  $M$ ,  $Z$ , and  $K$  in equation (1a).

Via recasting the aerodynamic parts of matrices  $\mathcal{A}$ ,  $\mathcal{B}$ , and  $\mathcal{C}$  will ultimately correspond to matrix  $Q(k)$  in equation (1a). The aerodynamic part of matrix  $\mathcal{A}$  contains noncirculatory aerodynamic terms only, sometimes referred to as apparent mass terms

$$\mathcal{A}_{non} = \kappa \begin{bmatrix} (\frac{1}{8}+a^2) & -(c-a)\frac{T_1}{\pi} - \frac{T_7}{\pi} & -\frac{a}{b} \\ -(c-a)\frac{T_1}{\pi} - \frac{T_7}{\pi} & -\frac{T_3}{\pi^2} & -\frac{T_1}{\pi b} \\ -a & -\frac{T_1}{\pi} & \frac{1}{b} \end{bmatrix}. \quad (3c)$$

There are no circulatory aerodynamic terms in matrix  $\mathcal{A}$

$$\mathcal{A}_{circ} = \begin{bmatrix} 0 & 0 & 0 \\ 0 & 0 & 0 \\ 0 & 0 & 0 \end{bmatrix}. \quad (3d)$$

Matrix  $\mathcal{B}$  contains aerodynamic terms only, both noncirculatory and circulatory

$$\mathcal{B}_{non} = \kappa \frac{v}{b} \begin{bmatrix} (\frac{1}{2}-a) & \frac{1}{\pi}(-2p - (\frac{1}{2}-a)T_4) & 0 \\ \frac{1}{\pi}(p - T_1 - \frac{T_4}{2}) & -\frac{1}{2\pi^2}T_4T_{11} & 0 \\ 1 & -\frac{1}{\pi}T_4 & 0 \end{bmatrix}, \quad (4c)$$

$$\mathcal{B}_{circ} = C(k) \kappa \frac{v}{b} \begin{bmatrix} 2(a^2 - \frac{1}{4}) & -\frac{1}{\pi}(a + \frac{1}{2})T_{11} & -2\frac{1}{b}(a + \frac{1}{2}) \\ \frac{1}{\pi}(\frac{1}{2} - a)T_{12} & \frac{1}{2\pi^2}T_{11}T_{12} & \frac{1}{b\pi}T_{12} \\ 2(\frac{1}{2} - a) & \frac{1}{\pi}T_{11} & 2\frac{1}{b} \end{bmatrix}. \quad (4d)$$

The aerodynamic part of matrix  $\mathcal{C}$  also contains both noncirculatory and circulatory terms

$$\mathcal{C}_{non} = \kappa \left(\frac{v}{b}\right)^2 \begin{bmatrix} 0 & \frac{1}{\pi}(T_4 + T_{10}) & 0 \\ 0 & \frac{1}{\pi^2}(T_5 - T_4T_{10}) & 0 \\ 0 & 0 & 0 \end{bmatrix}, \quad (5c)$$

$$\mathcal{C}_{circ} = C(k) \kappa \left(\frac{v}{b}\right)^2 \begin{bmatrix} -2(a + \frac{1}{2}) & -2\frac{1}{\pi}(a + \frac{1}{2})T_{10} & 0 \\ \frac{1}{\pi}T_{12} & \frac{1}{\pi^2}T_{10}T_{12} & 0 \\ 2 & 2\frac{1}{\pi}T_{10} & 0 \end{bmatrix}. \quad (5d)$$

Employing these constituent matrices and eliminating the null matrices  $\mathcal{A}_{circ}$  and  $\mathcal{B}_{struct}$ , equation (2a) may now be expressed as

$$\begin{aligned} & [\mathcal{A}_{struct}]\{\ddot{q}\} + [\mathcal{C}_{struct}]\{q\} \\ & + [\mathcal{A}_{non}]\{\ddot{q}\} + [\mathcal{B}_{non}]\{\dot{q}\} + [\mathcal{B}_{circ}]\{\dot{q}\} + [\mathcal{C}_{non}]\{q\} + [\mathcal{C}_{circ}]\{q\} = 0. \end{aligned} \quad (2b)$$

Recalling the purpose of comparing TAFs and GAFs, attention is now turned to the aerodynamic terms in equations (1a) and (2b). In equation (1a), the product  $\frac{1}{2}\rho v^2 [Q(k)]\{q\}$  corresponds, in equation (2b), to the sum of products  $[\mathcal{A}_{non}]\{\ddot{q}\}$ ,  $[\mathcal{B}_{non}]\{\dot{q}\}$ ,  $[\mathcal{B}_{circ}]\{\dot{q}\}$ ,  $[\mathcal{C}_{non}]\{q\}$ , and  $[\mathcal{C}_{circ}]\{q\}$ . However, there is a ‘‘mismatch’’ between the aerodynamic terms in equations (1a) and (2b): The sum in equation (2b) contains products of coefficient matrices with vector  $q$  and the time derivatives of  $q$  while the term in equation (1a) contains a product of a coefficient matrix and vector  $q$  only. This mismatch is resolved in the final step of the recasting.

**Step three.** – The third step is to employ the Fourier transform to express equations (1a) and (2b) in the frequency domain. Recall that the Fourier transforms of the first and second time derivatives of a quantity are equal, respectively, to  $i\omega$  times the Fourier transform of the quantity and  $(i\omega)^2$  times the Fourier transform of the quantity.

Recognizing that  $i\omega = ik\frac{v}{b}$  and that  $(i\omega)^2 = \left(ik\frac{v}{b}\right)^2 = -k^2\left(\frac{v}{b}\right)^2$ , equations (1a) and (2b) take the forms

$$-k^2\left(\frac{v}{b}\right)^2 [M]\{q\} + ik\frac{v}{b}[Z]\{q\} + [K]\{q\} + \frac{1}{2}\rho v^2[Q(k)]\{q\} = 0 \quad (1b)$$

and

$$\begin{aligned} & -k^2\left(\frac{v}{b}\right)^2 [\mathcal{A}_{struct}]\{q\} + [\mathcal{C}_{struct}]\{q\} \\ & -k^2\left(\frac{v}{b}\right)^2 [\mathcal{A}_{non}]\{q\} + ik\frac{v}{b}[\mathcal{B}_{non}]\{q\} + ik\frac{v}{b}[\mathcal{B}_{circ}]\{q\} + [\mathcal{C}_{non}]\{q\} + [\mathcal{C}_{circ}]\{q\} = 0. \end{aligned} \quad (2c)$$

Theodorsen's AEOM are now in the necessary form. All matrices in equations (1b) and (2c) are multiplied by vector  $q$ , thus removing the mismatch and making it possible to equate directly the aerodynamic terms in equation (2c) to the aerodynamic terms in equation (1b), or

$$\frac{1}{2}\rho v^2[Q(k)] = -k^2\left(\frac{v}{b}\right)^2 [\mathcal{A}_{non}] + ik\frac{v}{b}[\mathcal{B}_{non}] + ik\frac{v}{b}[\mathcal{B}_{circ}] + [\mathcal{C}_{non}] + [\mathcal{C}_{circ}]. \quad (6)$$

The elements of matrix  $Q(k)$  are Theodorsen's aerodynamic forces, examined next.

#### IV. ANALYTICAL EXPRESSIONS FOR THEODORSEN'S AERODYNAMIC FORCES

The goal of this section is to obtain analytical expressions for Theodorsen's aerodynamic forces (TAFs), which requires the examination of the right side of equation (6). Each matrix in equation (6) is order 3x3, with the rows corresponding to aerodynamic moments about the elastic axis, aerodynamic moments about the aileron hinge, and aerodynamic forces on the entire wing in the vertical direction, and with the columns corresponding to unit changes in torsion angle, aileron deflection angle, and vertical deflection.

As equation (6) specifies, the elements of matrix  $Q(k)$ , the TAFs, are obtained by performing the operations indicated on the right side. Thus, taking into account both the matrix coefficients on the right side of equation (6) and the elements of these matrices themselves (as found in eqns. (3c), (4c), (4d), (5c), and (5d)), the resulting expressions for the TAFs will be complex functions of reduced frequency.

Without showing at this time the full expressions for the TAFs, each matrix element of equation (6) has the form

$$\frac{1}{2}\rho v^2 Q_{ij}(k) = \kappa\left(\frac{v}{b}\right)^2 \{\mathbb{k}_{ij}[\mathbb{R}_{ij} + i\mathbb{I}_{ij}]\}. \quad (7)$$

Within the square brackets the real and imaginary components,  $\mathbb{R}_{ij}$  and  $\mathbb{I}_{ij}$ , are functions of reduced frequency, Theodorsen's circulation function, and the geometric quantities  $a$  and  $c$ . The constant  $\mathbb{k}_{ij}$  is element-specific and may be  $\frac{1}{\pi}$ ,  $\frac{1}{\pi^2}$ ,  $\frac{1}{b}$ ,  $\frac{1}{\pi b}$ , or 1.

In equation (7) if one substitutes the definition of  $\kappa$  into the multiplying factor,  $\kappa\left(\frac{v}{b}\right)^2$ , one obtains

$$\kappa\left(\frac{v}{b}\right)^2 = \frac{\pi\rho b^2}{M}\left(\frac{v}{b}\right)^2 = \frac{\pi\rho v^2}{M} = \left(\frac{2\pi}{M}\right)\frac{1}{2}\rho v^2.$$



Thus, both sides of equation (7) contain dynamic pressure, which may be eliminated, leaving

$$Q_{ij}(k) = \frac{2\pi}{M} \kappa_{ij} [\Re_{ij} + i\Im_{ij}]. \quad (8)$$

The multiplying factor in equation (7),  $\kappa \left(\frac{v}{b}\right)^2$ , is an artifact of the normalization Theodorsen chose in creating equations (A), (B), and (C). Thus, as explicitly indicated in equation (8), Theodorsen's normalization is responsible for the mass,  $M$ , appearing in every element of matrix  $Q(k)$ .

When the real and imaginary parts of the Theodorsen circulation function,  $F(k)$  and  $G(k)$ , are substituted for  $C(k)$ , the real and imaginary parts of matrix  $Q(k)$ , by column, are listed below. For simplicity,  $Q(k)$ ,  $F(k)$  and  $G(k)$  are written without their functional argument.

First column:

$$Q_{11_{Real}} = \frac{2\pi}{M} \left[ -\left(\frac{1}{8} + a^2\right)k^2 - 2\left(a^2 - \frac{1}{4}\right)Gk - 2\left(a + \frac{1}{2}\right)F \right]; \quad (9a)$$

$$Q_{11_{Imag}} = \frac{2\pi}{M} \left[ \left(\frac{1}{2} - a\right)k + 2\left(a^2 - \frac{1}{4}\right)Fk - 2\left(a + \frac{1}{2}\right)G \right]; \quad (9b)$$

$$Q_{21_{Real}} = \frac{2\pi}{M} \frac{1}{\pi} \left[ (T_7 + (c - a)T_1)k^2 - T_{12} \left(\frac{1}{2} - a\right)Gk + T_{12}F \right]; \quad (9c)$$

$$Q_{21_{Imag}} = \frac{2\pi}{M} \frac{1}{\pi} \left[ \left(p - T_1 - \frac{T_4}{2}\right)k + T_{12} \left(\frac{1}{2} - a\right)Fk + T_{12}G \right]; \quad (9d)$$

$$Q_{31_{Real}} = \frac{2\pi}{M} \left[ ak^2 - 2\left(\frac{1}{2} - a\right)Gk + 2F \right]; \quad (9e)$$

$$Q_{31_{Imag}} = \frac{2\pi}{M} \left[ k + 2\left(\frac{1}{2} - a\right)Fk + 2G \right]. \quad (9f)$$

Second column:

$$Q_{12_{Real}} = \frac{2\pi}{M} \frac{1}{\pi} \left[ (T_7 + (c - a)T_1)k^2 + (T_4 + T_{10}) + \left(a + \frac{1}{2}\right)T_{11}Gk - 2\left(a + \frac{1}{2}\right)T_{10}F \right]; \quad (9g)$$

$$Q_{12_{Imag}} = \frac{2\pi}{M} \frac{1}{\pi} \left[ -\left(2p + \left(\frac{1}{2} - a\right)T_4\right)k - \left(a + \frac{1}{2}\right)T_{11}Fk - 2\left(a + \frac{1}{2}\right)T_{10}G \right]; \quad (9h)$$

$$Q_{22_{Real}} = \frac{2\pi}{M} \frac{1}{\pi^2} \left[ T_3k^2 + (T_5 - T_4T_{10}) - \frac{T_{11}T_{12}}{2}Gk + T_{10}T_{12}F \right]; \quad (9i)$$

$$Q_{22_{Imag}} = \frac{2\pi}{M} \frac{1}{\pi^2} \left[ -\frac{T_4T_{11}}{2}k + \frac{T_{11}T_{12}}{2}Fk + T_{10}T_{12}G \right]; \quad (9j)$$

$$Q_{32_{Real}} = \frac{2\pi}{M} \frac{1}{\pi} \left[ T_1k^2 - T_{11}Gk + 2T_{10}F \right]; \quad (9k)$$

$$Q_{32_{Imag}} = \frac{2\pi}{M} \frac{1}{\pi} \left[ -T_4k + T_{11}Fk + 2T_{10}G \right]. \quad (9l)$$

Third column:

$$Q_{13_{Real}} = \frac{2\pi}{M} \frac{1}{b} \left[ ak^2 + 2 \left( a + \frac{1}{2} \right) Gk \right]; \quad (9m)$$

$$Q_{13_{Imag}} = \frac{2\pi}{M} \frac{1}{b} \left[ -2 \left( a + \frac{1}{2} \right) Fk \right]; \quad (9n)$$

$$Q_{23_{Real}} = \frac{2\pi}{M} \frac{1}{\pi b} [T_1 k^2 - T_{12} Gk]; \quad (9o)$$

$$Q_{23_{Imag}} = \frac{2\pi}{M} \frac{1}{\pi b} [T_{12} Fk]; \quad (9p)$$

$$Q_{33_{Real}} = \frac{2\pi}{M} \frac{1}{b} [-k^2 - 2Gk]; \quad (9q)$$

$$Q_{33_{Imag}} = \frac{2\pi}{M} \frac{1}{b} [2Fk]. \quad (9r)$$

The elements of matrix  $Q(k)$ , equations (9a) through (9r), are analogous to the generalized aerodynamic forces (GAFs) produced by the doublet lattice method.

It should be noted that Fung (ref. 5), Hodges and Pierce (ref. 6), Wright and Cooper (ref. 7), and Weisshaar (ref. 8) all present, in various forms, expressions that are analogous to equations (9a) and (9b), (9e) and (9f), (9m) and (9n), and (9q) and (9r). The expressions in references 5-8 correspond to a typical section without an aileron; there are no expressions in these references corresponding to a typical section with an aileron.

## V. APPROXIMATING A TYPICAL SECTION USING THE DLM

The DLM was chosen for computing GAFs because it is so commonly used in the field of Aeroelasticity.

In order to compare the TAFs and GAFs in a meaningful way, it is necessary to recognize and attempt to minimize the fundamental differences between TAFs and GAFs:

TAFs are aerodynamic forces for a typical section (i.e., a two-dimensional wing) in incompressible flow;

GAFs from the DLM are aerodynamic forces for a three-dimensional wing in compressible subsonic flow.

To minimize these differences, it was necessary, therefore, to create a doublet lattice model whose aerodynamics would reasonably approximate the aerodynamics of a typical section in incompressible flow, discussed next.

The three-dimensional analog of a typical section with a trailing-edge control surface is an unswept rectangular wing of infinite span with a trailing-edge control surface, also of infinite span. Such a wing and control surface would produce chordwise pressure distributions that are invariant as one proceeds out the span.

The DLM analog of incompressible flow is a flow whose Mach number is zero. Such a flow would have characteristics equivalent to those assumed by Theodorsen in reference 2.

However, a DLM aerodynamic model with infinite span at any Mach number is impossible to construct and, thus, the corresponding GAFs impossible to compute. It was assumed that a DLM aerodynamic model with a very high aspect ratio unswept rectangular wing at zero Mach number would sufficiently minimize the differences so that a meaningful comparison could be made. If these assumptions are correct, chordwise pressure distributions for the inboard portion of the wing would be almost invariant as one proceeds out the span. Thus, GAFs computed using only the pressures and mode shapes from the inboard 10 percent of the wing semispan should approximate, as well as can be expected, GAFs for a typical section in incompressible flow.

To this end, an unswept rectangular wing with an aspect ratio of 20 at zero Mach number was chosen for the DLM aerodynamic model. The DLM has an option to take advantage of symmetry (or asymmetry) and to model only half of the configuration. Employing this option, the aspect ratio of the half wing was 10. Figure 2 shows a sketch of the aerodynamic model. Appendix B describes this aerodynamic model in detail and addresses the validity of the high-aspect-ratio assumption.

## VI. CALCULATION OF TAFs AND GAFs

The calculations described in this section of the paper were performed with quantities corresponding to the “standard case” in reference 2:

$$\kappa = 0.1; c = 0.5; a = -0.4; x_\alpha = 0.2; r_\alpha^2 = 0.25; x_\beta = \frac{1}{80}; r_\beta^2 = \frac{1}{160}; b = 1;$$

with frequencies,  $\omega_\alpha$ ,  $\omega_\beta$ , and  $\omega_h$ , variable.

But because the TAFs and GAFs deal with aerodynamic forces only and not structural forces, the quantities  $a$  and  $c$  are the only ones from the standard case necessary for the calculations.

TAFs were computed in Matlab® using equations (9a) through (9r). The quantity  $\frac{2\pi}{M}$  was set to unity. These equations were solved for 101 values of reduced frequency beginning at  $1 \times 10^{-6}$  with an increment of 0.01, for an effective range of 0 to 1. (The first reduced frequency was not zero for the following reason: In Matlab® at zero reduced frequency, Bessel functions of the second kind – elements appearing in both the numerator and denominator of the real and imaginary parts of Theodorsen’s circulation function – assume values of minus infinity, which, in turn, cause these same real and imaginary parts to be “not a number,” i.e., an undefined or not-representable value.)

The GAFs were computed in the version of the doublet lattice method residing in the ISAC code (ref. 9) using the aerodynamic model described in the previous section. The analysis included degrees of freedom of pitch, trailing-edge control surface deflection, and plunge (analogous to torsion, aileron deflection, and vertical deflection for the TAFs). To better approximate a pressure distribution invariant with span, only the inboard 20 strips of the DLM aerodynamic model were used to compute the GAFs. The pitch axis was set at 30% chord (equivalent to  $a = -0.4$ ) and the trailing-edge control surface hinge was set at 75% chord (equivalent to  $c = 0.5$ ). The doublet lattice model was executed for 12 values of reduced frequency ranging from 0 to 1.

Before plotting, each TAF and each GAF was normalized by its own maximum complex absolute value over its own range of reduced frequencies. This normalization removed the differences in absolute magnitudes of the TAFs and GAFs due to dimensional factors within equations (9a) through (9r) and within the DLM, leaving only the general shapes and normalized amplitudes of the TAFs and GAFs for comparison.

Figure 3 contains nine plots arranged in three rows and three columns. The TAFs are indicated by solid lines and the GAFs by open circles. In each plot, the imaginary part of the TAF or GAF is plotted as a function of its respective real part. The arrows indicate the direction of increasing reduced frequency. An indexed pair,  $(i,j)$ , identifies each plot. The first index in the pair specifies an aerodynamic force or moment ( $i = 1$  refers to torsion moment;  $i = 2$  refers to aileron hinge moment;  $i = 3$  refers to vertical force) and the second index specifies a unit displacement in one of the degrees of freedom ( $j = 1$  refers to torsion or pitch;  $j = 2$  refers to aileron deflection;  $j = 3$  refers to vertical deflection or plunge).

Referring back to the normalization of the computed TAFs and GAFs, mentioned above, these particular TAFs and GAFs are always normalized by either their first point (at  $k = 0$ ) or their last point (at  $k = 1$ ). In eight of the nine cases presented in figure 3 the normalizing point for a given TAF corresponds to the normalizing point for the companion GAF; that is, either both normalizing points are at  $k = 0$  or both normalizing points are at  $k = 1$ . However, this is not the situation for the (3,1) case; in this case the TAF is normalized by its point at  $k = 0$  while this GAF is normalized by its point at  $k = 1$ . The magnitude difference between the (3,1) TAF and the (3,1) GAF along the real axis near a real part of unity is the result of this normalization quirk.

From a qualitative perspective, the magnitudes and shapes of corresponding TAFs and GAFs in figure 3 agree very well. The next section of the paper examines quantitative comparisons of the TAFs and GAFs.

## VII. COMPARISON OF TAFs AND GAFs

This section of the paper presents quantitative comparisons of the magnitudes and shapes of corresponding TAFs and GAFs.

### Comparison of Magnitudes

The percentage difference between the complex absolute values of each pair of normalized TAFs and GAFs at a single reduced frequency ( $k = 0.5$ ) was chosen as the measure for comparing magnitudes. While this quantity is not a definitive measure of the magnitude differences between TAFs and GAFs (percentage differences will vary depending on the reduced frequency chosen), because  $k = 0.5$  is the middle value in the range of reduced frequencies, it is nonetheless thought to be a representative measure. The adjectives “good,” “very good,” and “excellent” are used to describe differences in magnitude ranging from 10 to five percent, five to one percent, and less than one percent, respectively.

The percentage differences were computed with the following results:

**TABLE 1. – SIMILARITY IN MAGNITUDE FOR PAIRS OF TAFs AND GAFs**

<b>Percentage Differences Between Complex Absolute Values at <math>k = 0.5</math></b>			
	<b><math>i = 1</math></b>	<b><math>i = 2</math></b>	<b><math>i = 3</math></b>
<b><math>j = 1</math></b>	0.57	0.88	1.16
<b><math>j = 2</math></b>	0.57	1.91	0.70
<b><math>j = 3</math></b>	2.56	6.76	0.87

where indices  $i$  and  $j$  are elements of the indexed pair defined in Section VI of this paper.

As can be seen from Table 1, the percentage differences in magnitudes between corresponding pairs of TAFs and GAFs are generally very small, with most differences less than one percent, suggesting good-to-excellent agreement in the magnitudes of the normalized TAFs and GAFs. The average percentage differences are largest for the second column (corresponding to aileron deflection) and quantify what the eye clearly sees in figure 3: there is more separation between the circles and the solid lines in the second column than in the other two columns. Not quantified in Table 1, but apparent from visual examination of figure 3, is that for all corresponding pairs of TAFs and GAFs their respective starting and ending values, maxima and minima, and sign changes (if present) are also in very good agreement.

### **Comparison of Shapes**

An ordinary Procrustes analysis (OPA, ref. 10) is a means of quantifying the similarity in the shapes of two curves. An OPA was performed for each pair of normalized TAFs and GAFs as they appear in figure 3. A requirement of an OPA is that each shape be defined by the same number of points. Therefore, from the full set of 101 points defining each TAF, subsets of 12 points were created that correspond to the 12 reduced frequencies defining each GAF, where each “point” is a point in the complex plane defined by a real part and an imaginary part.

An OPA is a three-step process:

- (1) the translation of the centroid of each shape to the origin (in this case the origin of the complex plane);
- (2) the scaling of each translated shape so that the root mean square distance (RMSD) of its points to the origin is unity; and
- (3) the optimal rotation of one translated and scaled shape so as to minimize the sum of the squared distances (SSD) between corresponding points of the two translated and scaled shapes.

At the completion of these steps, the two curves have been translated (so that their centroids are coincident at the origin), scaled (so that they are “the same size”), and optimally rotated (so that corresponding points on the two curves are “as close as they can be” to each other). At this stage in the process, a single quantitative measure can be computed that captures the similarity in the shapes of the two curves. This quantitative measure is the square root of the minimized SSD obtained from step (3) and is referred to as the “Procrustes distance.” The smaller the Procrustes distance, the better the similarity between shapes. A Procrustes distance of zero indicates identical shapes.

The Procrustes distance is a relative measure that is a function of the number of points defining each curve. Two curves defined by a given number of points will have a correspondingly larger Procrustes distance than the same two curves defined by fewer points.

As a reference, Procrustes distances were computed for three pairs of curves unrelated to TAFs and GAFs: one pair with dissimilar shapes (semicircle and line segment); another pair with similar shapes (semicircle and semi-ellipse with an eccentricity of 0.886); and a final pair with identical shapes (two line segments with different locations, lengths, and orientations). So that these Procrustes distances would be consistent with those for the TAFs and GAFs, these curves were also described by 12 points each. Results for these pairs of curves are summarized in Table 2:

**TABLE 2. – SIMILARITY IN SHAPE FOR VARIOUS PAIRS OF CURVES**

Shapes (as defined above)	Procrustes Distances
Dissimilar	1.71
Similar	0.806
Identical	0

Based on the results in Table 2, the adjectives “good,” “very good,” and “excellent” are used to describe differences in Procrustes distances ranging from 0.403 to 0.2, 0.2 to 0.1, and less than 0.1, respectively.

For the pairs of TAFs and GAFs, the resulting Procrustes distances are summarized in Table 3:

**TABLE 3. – SIMILARITY IN SHAPE FOR PAIRS OF TAFs AND GAFs**

Procrustes Distances for -			
	<i>i</i> = 1	<i>i</i> = 2	<i>i</i> = 3
<i>j</i> = 1	0.0455	0.0625	0.0242
<i>j</i> = 2	0.0394	0.0527	0.0086
<i>j</i> = 3	0.1544	0.2813	0.0191

where indices *i* and *j* are elements of the indexed pair defined in Section VI of this paper.

All Procrustes distances in Table 3 lie between those for the similar and identical shapes in Table 2, with most Procrustes distances in Table 3 at least an order of magnitude smaller than unity. These results indicate that the shapes of the TAFs and the shapes of the GAFs are in good-to-excellent agreement with each other. The TAFs and GAFs whose Procrustes distances are the smallest, and therefore, whose shapes are most similar, are those for *i* = 3 (aerodynamic forces due to flexure), followed by those for *i* = 1 (aerodynamic forces due to torsion), followed by those for *i* = 2 (aerodynamic forces due to aileron deflection). Not quantified in Table 3, but apparent from visual examination of figure 3, is that for all corresponding pairs of TAFs and GAFs their respective curvatures and inflection points are also in very good agreement.

### VIII. RELATIONSHIPS AMONG THE TAFs

As stated in Section IV of this paper, the elements of matrix  $Q(k)$ , equations (9a) through (9r), are analogous to the generalized aerodynamic forces (GAFs) produced by the doublet lattice method and figure 3 and Tables 1 and 3 confirm the extent to which this is true. To distinguish the TAFs from the GAFs, for purposes of the following discussion, the GAFs are assigned the symbol  $\tilde{Q}$ .

In the classical aeroelastic equations of motion, when the rigid-body modes are pure plunge ( $h$ ) and pure pitch ( $\alpha$ ), it is possible to extract some of the longitudinal stability derivatives from the GAFs produced by the DLM (refs. 11 and 12). Two such derivatives, the lift curve slope and the static stability derivative, may each be obtained in two different ways: The first is from the real part of the generalized force or moment due to  $\alpha$  at zero reduced frequency; the second is from the imaginary part of the generalized force or moment due to  $h$  at a very small value of reduced frequency. Using Theodorsen's mode-ordering convention, these expressions are

$$C_{L\alpha} = -\frac{\tilde{Q}_{31Real}}{S} = -\frac{\tilde{Q}_{33Imag}\bar{c}}{2Sk} \quad (10a)$$

and

$$C_{m\alpha} = \frac{\tilde{Q}_{11Real}}{S\bar{c}} = \frac{\tilde{Q}_{13Imag}}{2Sk}. \quad (11a)$$

where  $S$  is wing area and  $\bar{c}$  is mean aerodynamic chord.

From equations (10a) and (11a), the following expressions follow:

$$\tilde{Q}_{31Real} = \tilde{Q}_{33Imag} \frac{\bar{c}}{2k}; \quad (10b)$$

and

$$\tilde{Q}_{11Real} = \tilde{Q}_{13Imag} \frac{\bar{c}}{2k}. \quad (11b)$$

If the quantity  $\bar{b}$  is defined to be  $\bar{b} = \frac{\bar{c}}{2}$ , then equations (10b) and (11b) become

$$\tilde{Q}_{31Real} = \tilde{Q}_{33Imag} \frac{\bar{b}}{k} \quad (10c)$$

and

$$\tilde{Q}_{11Real} = \tilde{Q}_{13Imag} \frac{\bar{b}}{k}. \quad (11c)$$

Flexure ( $h$ ) and torsion ( $\alpha$ ) in Theodorsen's aeroelastic equations of motion are related to plunge and pitch in the classical equations. The total force on the wing in the vertical direction in Theodorsen's equations is directly analogous to lift in the classical equations. The torsion moment in Theodorsen's equations is related, but not directly, to the pitching moment in the classical equations (the former is about the elastic axis, the latter is about the center of gravity).

With these close relationships between Theodorsen's and the classical aeroelastic equations of motion one would expect that the following analogous relationships among the TAFs, analogous to equations (10c) and (11c) for the GAFs, might also be true:

$$Q_{31_{Real}} = Q_{33_{Imag}} \frac{b}{k}; \quad (12a)$$

and

$$Q_{11_{Real}} = Q_{13_{Imag}} \frac{b}{k}. \quad (13a)$$

where, for a typical section, the mean aerodynamic semichord,  $\bar{b}$ , is its semichord,  $b$ .

This is, in fact, the case.

To prove that the right sides of equations (12a) and (13a) are equal to their respective left sides, equations (9e) and (9r) are substituted into equation (12a) and equations (9a) and (9n) are substituted into equation (13a), yielding

$$\frac{2\pi}{M} \left[ ak^2 - 2 \left( \frac{1}{2} - a \right) Gk + 2F \right] = \frac{2\pi}{M} \frac{1}{b} [2Fk] \frac{b}{k} \quad (12b)$$

and

$$\frac{2\pi}{M} \left[ - \left( \frac{1}{8} + a^2 \right) k^2 - 2 \left( a^2 - \frac{1}{4} \right) Gk - 2 \left( a + \frac{1}{2} \right) F \right] = \frac{2\pi}{M} \frac{1}{b} \left[ -2 \left( a + \frac{1}{2} \right) Fk \right] \frac{b}{k}, \quad (13b)$$

respectively.

Recall that equations (10a) through (13b) hold only when their left sides are evaluated at zero reduced frequency and their right sides are evaluated at very small values of reduced frequency. At zero reduced frequency, within the left sides of equations (12b) and (13b), the terms containing  $k$  and  $k^2$  are zero. When these terms are eliminated from the left sides of equations (12b) and (13b) and the factor  $\frac{2\pi}{M}$  is removed from both sides, equations (12b) and (13b) become

$$[2F] = \frac{1}{b} [2Fk] \frac{b}{k}, \quad (12c)$$

which is an identity, and

$$\left[ -2 \left( a + \frac{1}{2} \right) F \right] = \frac{1}{b} \left[ -2 \left( a + \frac{1}{2} \right) Fk \right] \frac{b}{k}, \quad (13c)$$

which is also an identity.

Although not shown in references 11 and 12, a relationship similar to those expressed in equations (12a) and (13a) also exists between the real part of Theodorsen's aerodynamic aileron hinge moment due to  $\alpha$ ,  $Q_{21_{Real}}$ , and the imaginary part of Theodorsen's aerodynamic aileron hinge moment due to  $h$ ,  $Q_{23_{Imag}}$ , namely

$$Q_{21_{Real}} = Q_{23_{Imag}} \frac{b}{k}. \quad (14a)$$



When equations (9c) and (9p) are substituted into equation (14a), the following equation is obtained

$$\frac{2\pi}{M} \frac{1}{\pi} \left[ (T_7 + (c - a)T_1)k^2 - T_{12} \left( \frac{1}{2} - a \right) Gk + T_{12}F \right] = \frac{2\pi}{M} \frac{1}{\pi} \frac{1}{b} [T_{12}Fk] \frac{b}{k}. \quad (14b)$$

And, again, when the terms containing  $k$  and  $k^2$  on the left side are set to zero and the factor  $\frac{2\pi}{M}$  is removed from both sides, equation (14b) becomes

$$\frac{1}{\pi} [T_{12}F] = \frac{1}{\pi} \frac{1}{b} [T_{12}Fk] \frac{b}{k}, \quad (14c)$$

which, again, is an identity.

Thus, as confirmed by the identities in equations (12c), (13c), and (14c), the relationships between the real parts of aerodynamic forces or moments due to  $\alpha$  at zero reduced frequency and the imaginary parts of those same forces or moments due to  $\dot{h}$  at a very small value of reduced frequency that held for the GAFs from the DLM also hold for the TAFs from Theodorsen's aeroelastic equations of motion.

## IX. CONCLUDING REMARKS

This paper has investigated the similarity between the unsteady aerodynamic forces and moments derived in reference 2 (termed herein "Theodorsen's aerodynamic forces," or TAFs) and the generalized aerodynamic forces (GAFs) computed by the doublet lattice method (DLM) (ref. 3). Some of the important conclusions are:

- (1) Analytical expressions for the TAFs were extracted from Theodorsen's aeroelastic equations of motion.
- (2) A comparison of normalized TAFs and GAFs for the "standard case" of reference 2 indicated good-to-excellent agreement in magnitudes and shapes.
- (3) Relationships between selected pairs of analytical expressions for the TAFs were shown to be identical to known analogous expressions between corresponding pairs of GAFs.
- (4) The averaged incremental chordwise pressure distributions for the inboard ten percent semispan of a very high aspect ratio (AR = 20) rectangular wing at zero Mach number are good approximations to corresponding pressures for a typical section in incompressible flow.

**APPENDIX A**  
**THEODORSEN'S CIRCULATION FUNCTION**

In reference 2, Theodorsen derives a function that has been associated with his name for over three-quarters of a century, Theodorsen's circulation function,  $C(k)$ , a complex function of reduced frequency with real part  $F(k)$  and imaginary part  $G(k)$ , expressed in equation (A1):

$$C(k) = F(k) + iG(k). \quad (A1)$$

In terms of equations (A), (B), and (C) in the main body of this paper,  $C(k)$  determines the magnitude attenuations and and phase lags in circulatory aerodynamic forces and moments due to variations in torsion, aileron deflection, and flexure for a typical section in unsteady incompressible potential flow.

Theodorsen's circulation function may be expressed in terms of Bessel functions of the first and second kinds,  $J_i(k)$  and  $Y_i(k)$ , respectively, where subscript  $i$  denotes the order of the Bessel function. As expressed in reference 2, the real part of  $C(k)$  is

$$F(k) = \frac{J_1(k)[J_1(k) + Y_0(k)] + Y_1(k)[Y_1(k) - J_0(k)]}{[J_1(k) + Y_0(k)]^2 + [Y_1(k) - J_0(k)]^2} \quad (A2)$$

and the imaginary part is

$$G(k) = -\frac{Y_1(k)Y_0(k) + J_1(k)J_0(k)}{[J_1(k) + Y_0(k)]^2 + [Y_1(k) - J_0(k)]^2}. \quad (A3)$$

Theodorsen's circulation function is presented graphically in three different forms, each form revealing different aspects of  $C(k)$ . All plots were generated in Matlab® by solving equations (A2) and (A3) for values of reduced frequency beginning at  $1 \times 10^{-6}$  and ending at 100. This first reduced frequency was not zero because, in Matlab®, Bessel functions of the second kind (appearing multiple times in eqns. (A2) and (A3)) assume values of minus infinity at zero reduced frequency.

Figure A1 presents the real part and the negative of the imaginary part of Theodorsen's circulation function as functions of reduced frequency. Both scales are linear. At  $k = 0$ , the value of  $F(k)$  is unity, but is seen to quickly drop off with increasing  $k$ , approaching a value of 0.5 as  $k$  approaches infinity. At  $k = 0$ , the value of  $G(k)$  is zero and approaches zero again as  $k$  approaches infinity.

Figure A2 presents Theodorsen's circulation function in frequency-response-function fashion. The upper plot contains the magnitude (complex absolute value) of  $C(k)$  as a function of reduced frequency; the lower plot contains the phase angle, expressed in degrees, as a function of reduced frequency. Both plots are semi-log, with the frequency scales logarithmic and covering four decades. It can be seen that the low- and high-frequency asymptotes of the magnitude are unity and 0.5, respectively, the low- and high-frequency asymptotes of the phase angle are both zero degrees, and that the maximum phase lag introduced is on the order of 15 degrees at a reduced frequency of about 0.3.

Figure A3 presents Theodorsen's circulation function in the complex plane with the imaginary part of  $C(k)$  plotted against its real part. Both scales are linear. Reduced frequency varies along the length of the curve and the arrow indicates the direction of increasing reduced frequency. Reduced frequencies of 0.01, 0.1, 1, and 10 are indicated by circles.

## **APPENDIX B**

### **DOUBLET LATTICE AERODYNAMIC MODEL**

This appendix describes the aerodynamic model from the doublet lattice method (DLM) constructed to compute the generalized aerodynamic forces (GAFs) for comparison with the Theodorsen aerodynamic forces (TAFs). This appendix also addresses the validity of the assumption made in Section V of the main body of this paper, namely that the steady pressures computed by the DLM for very high aspect ratio ( $AR = 20$ ) unswept rectangular wing at zero Mach number would approximate very well the theoretical steady pressures for a typical section. An implied assumption is that if the steady pressures agree, the unsteady pressures will as well.

#### **Doublet Lattice Method**

The DLM is a well-known and extensively-used linear finite-element unsteady aerodynamic code that is an extension of the vortex lattice method. Lifting surfaces are approximated by “segments of planes ... divided into small trapezoidal [boxes] ... arranged in columns parallel to the freestream” (ref. 3). Steady flow effects are represented by a horseshoe vortex located on each trapezoidal [box] and oscillatory flow increments are represented by a uniform line of acceleration potential doublets added to the bound vortices (ref. 3). The DLM has been used by many airplane manufacturers for many decades to predict the flutter characteristics of many airplanes in use today.

#### **Aerodynamic Model**

The number and distribution of boxes in a DLM aerodynamic model is highly dependent on the configuration being investigated. For the current configuration, a large number of boxes was necessary in the chordwise direction in order to capture the rapidly changing chordwise pressure distributions immediately aft of the wing leading edge and immediately forward and aft of the aileron hinge line. A large number of boxes was necessary in the spanwise direction due to the high aspect ratio of the wing. These necessities led to an aerodynamic model with a very large number of boxes.

Table B1 shows the box chordwise properties chosen for this aerodynamic model. There were 33 boxes in the chordwise direction with box chords smallest in regions where pressure changes are largest (near the wing leading edge and forward and aft of the aileron hinge). Box aspect ratios have an inverse relationship with box chords. To comply with box-aspect-ratio requirements, the aerodynamic model contained 200 strips, each with a width of five percent of the chord, producing a final aerodynamic model containing 6600 boxes. The model was comprised of two panels: one representing the forward portion of the wing, from the leading edge to the aileron hinge line; the other representing the full-span aileron, from the hinge line to the trailing edge. The shaded entries in Table B1 correspond to boxes on the aileron.

**TABLE B1. – CHORDWISE BOX PROPERTIES**  
Expressed as x/c

Box No.	Box LE	Box TE	Box Chord	Box AR	Box No.	Box LE	Box TE	Box Chord	Box AR
1	0.0000	0.0200	0.0200	2.5000	--	--	--	--	--
2	0.0200	0.0425	0.0225	2.2222	18	0.5785	0.6105	0.0320	1.5625
3	0.0425	0.0675	0.0250	2.0000	19	0.6105	0.6400	0.0295	1.6949
4	0.0675	0.0945	0.0270	1.8519	20	0.6400	0.6670	0.0270	1.8519
5	0.0945	0.1235	0.0290	1.7241	21	0.6670	0.6910	0.0240	2.0833
6	0.1235	0.1545	0.0310	1.6129	22	0.6910	0.7130	0.0220	2.2727
7	0.1545	0.1875	0.0330	1.5152	23	0.7130	0.7325	0.0195	2.5641
8	0.1875	0.2225	0.0350	1.4286	24	0.7325	0.7500	0.0175	2.8571
9	0.2225	0.2595	0.0370	1.3514	25	0.7500	0.7675	0.0175	2.8571
10	0.2595	0.2985	0.0390	1.2821	26	0.7675	0.7875	0.0200	2.5000
11	0.2985	0.3390	0.0405	1.2346	27	0.7875	0.8100	0.0225	2.2222
12	0.3390	0.3810	0.0420	1.1905	28	0.8100	0.8350	0.0250	2.0000
13	0.3810	0.4235	0.0425	1.1765	29	0.8350	0.8625	0.0275	1.8182
14	0.4235	0.4655	0.0420	1.1905	30	0.8625	0.8925	0.0300	1.6667
15	0.4655	0.5055	0.0400	1.2500	31	0.8925	0.9250	0.0325	1.5385
16	0.5055	0.5435	0.0380	1.3158	32	0.9250	0.9610	0.0360	1.3889
17	0.5435	0.5785	0.0350	1.4286	33	0.9610	1.0000	0.0390	1.2821

The reduced frequencies chosen for the doublet lattice aerodynamic model were 0, 0.05, 0.1, 0.2, 0.3, 0.4, 0.5, 0.6, 0.7, 0.8, 0.9, and 1.

#### Validity of High-Aspect-Ratio Assumption

As a check on the high-aspect-ratio assumption, at zero reduced frequency the chordwise pressures along strips 2 through 20 were compared with the chordwise pressures along the first strip. If the assumption is valid then, from corresponding box to corresponding box, pressures in strips 2 to 20 should be only minimally different from pressures in strip 1.

These comparisons were made. The pressures due to pitch for each box in strips 2 through 20 were found to be within 0.1% of their respective values for each box in strip 1; the pressures due to aileron deflection were within 0.2%. (At zero reduced frequency there is no pressure produced due to plunge.) Thus, over this portion of the wing, the chordwise pressure distributions are, in fact, near-invariant as one proceeds out the span and the high-aspect-ratio assumption is judged to be valid.

## REFERENCES

1. Perry, Boyd, III: *Recomputation of Numerical Results Contained in NACA Report No. 496*. NASA/TP-2015-218765, June 2015.
2. Theodorsen, Theodore: *General Theory of Aerodynamic Instability and the Mechanism of Flutter*. NACA Report No. 496, 1940.
3. Albano, Edward; and Rodden, William P.: *A Doublet-Lattice Method for Calculating Lift Distributions on Oscillating Surfaces in Subsonic Flows*. AIAA Journal. Vol. 7, No. 2, February 1969, pp. 279-285.
4. Hassig, Hermann J.: *An Approximate True Damping Solution of the Flutter Equation by Determinant Iteration*. Journal of Aircraft. Vol. 8, No. 11, November 1971, pp. 885-889.
5. Fung, Y. C.: *An Introduction to the Theory of Aeroelasticity*. Dover Publications, Inc., New York, 1969.
6. Hodges, Dewey H.; and Pierce, G. Alvin: *Introduction to Structural Dynamics and Aeroelasticity*. Cambridge University Press, New York, New York, 2002.
7. Wright, Jan R.; and Cooper, Jonathan E.: *Introduction to Aircraft Aeroelasticity and Loads*. John Wiley and Sons, Ltd., West Sussex, England, 2007.
8. Weisshaar, Terrence A.: *Lecture Notes from AAE 556, Aeroelasticity, Lectures 34-35*. Purdue University, West Lafayette, Indiana, 2011.
9. Peele, Elwood L.; and Adams, William M., Jr.: *Digital Program for Calculating the Interactions Between Flexible Structures, Unsteady Aerodynamics, and Active Controls*. NASA Technical Memorandum 80040, January 1979.
10. Anonymous: *Procrustes Analysis*. [https://en.wikipedia.org/wiki/Procrustes\\_analysis](https://en.wikipedia.org/wiki/Procrustes_analysis)
11. Rodden, William P.; and Giesing, Joseph P.: *Application of Oscillatory Aerodynamic Theory to Estimation of Dynamic Stability Derivatives*. Journal of Aircraft. Vol. 7, No. 3, May-June 1970, pp. 272-275.
12. Rodden, William P.; Bellinger, E. Dean; and Giesing, Joseph P.: *Errata and Addenda to "Application of Oscillatory Aerodynamic Theory to Estimation of Dynamic Stability Derivatives."* Journal of Aircraft. Vol. 21, No. 1, January 1984, pp. 93-94.

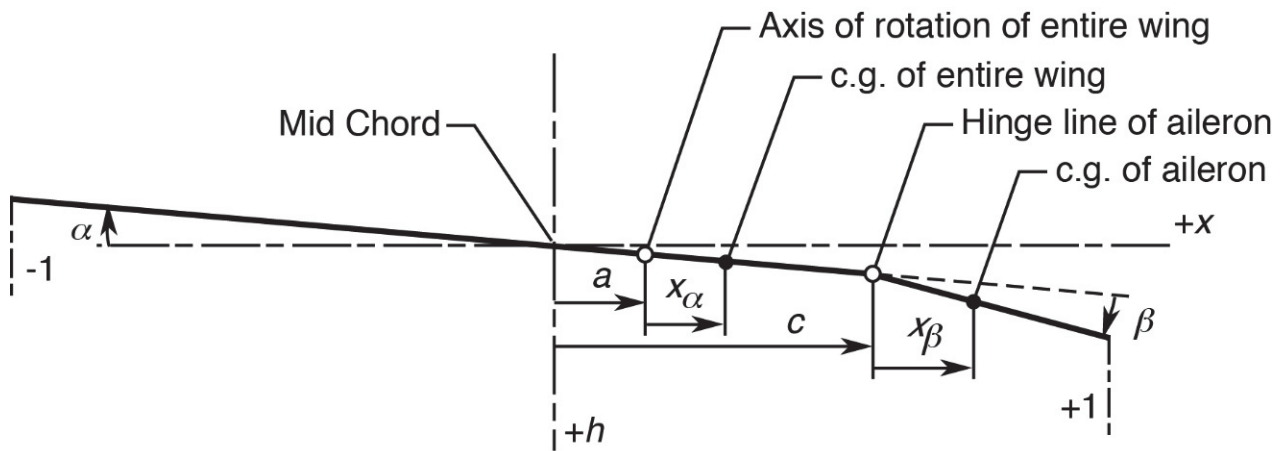


Figure 1. – Parameters of the airfoil-aileron combination

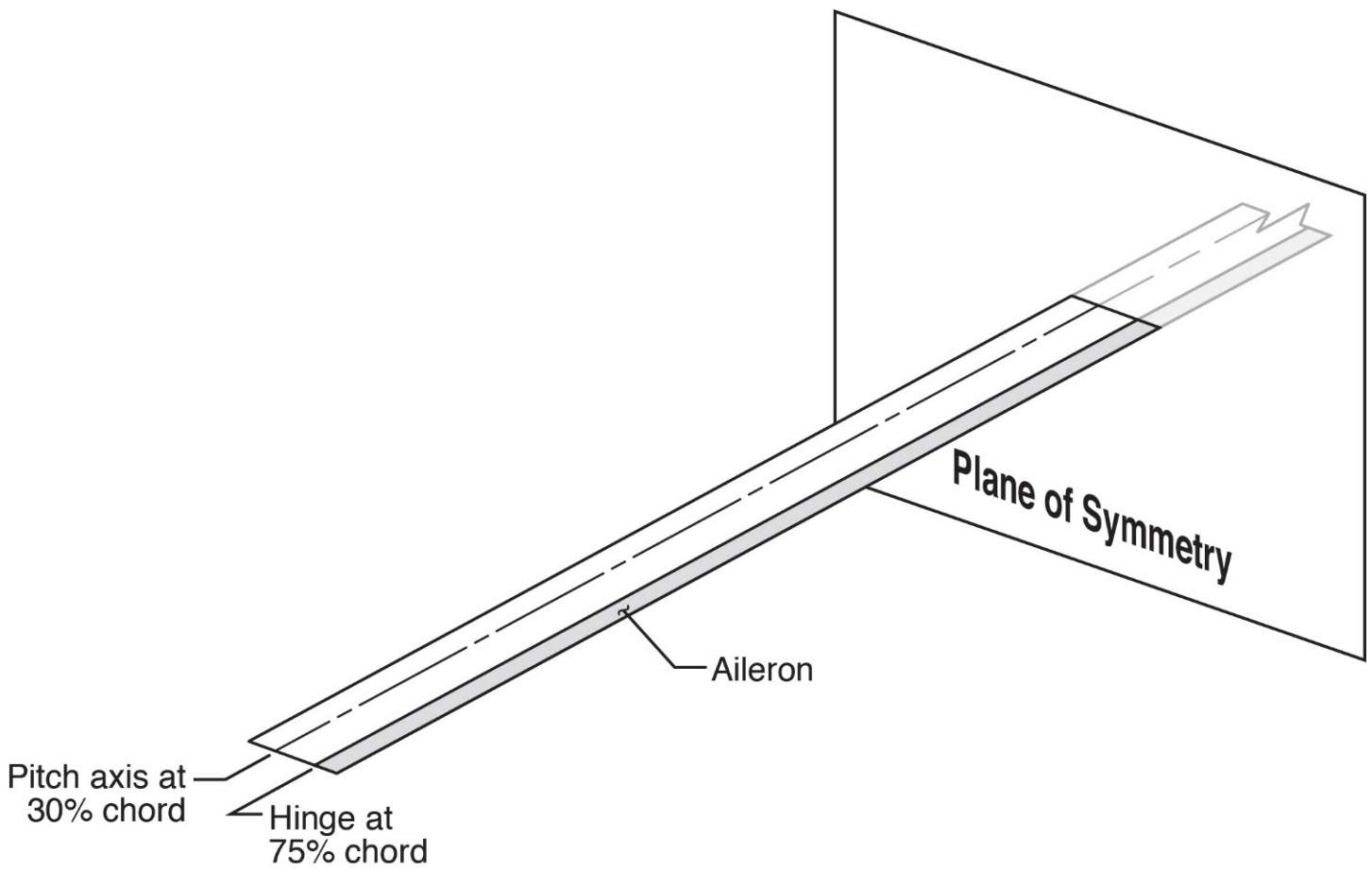


Figure 2. – Aerodynamic model of DLM very-high-aspect-ratio wing model.

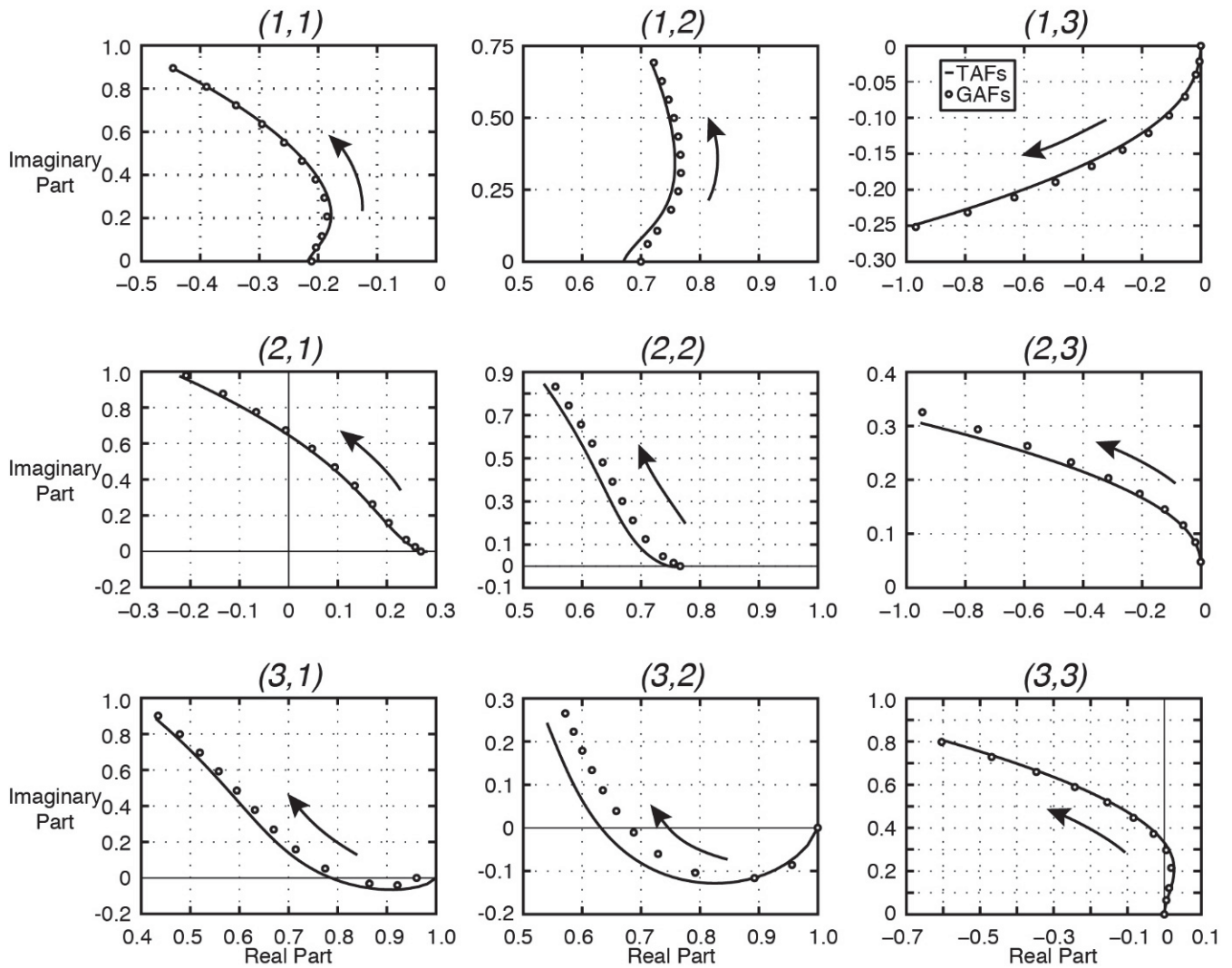


Figure 3. – Comparison of Theodorsen's aerodynamic forces from equation (9) and generalized aerodynamic forces from the doublet lattice method. Arrows indicate direction of increasing reduced frequency.



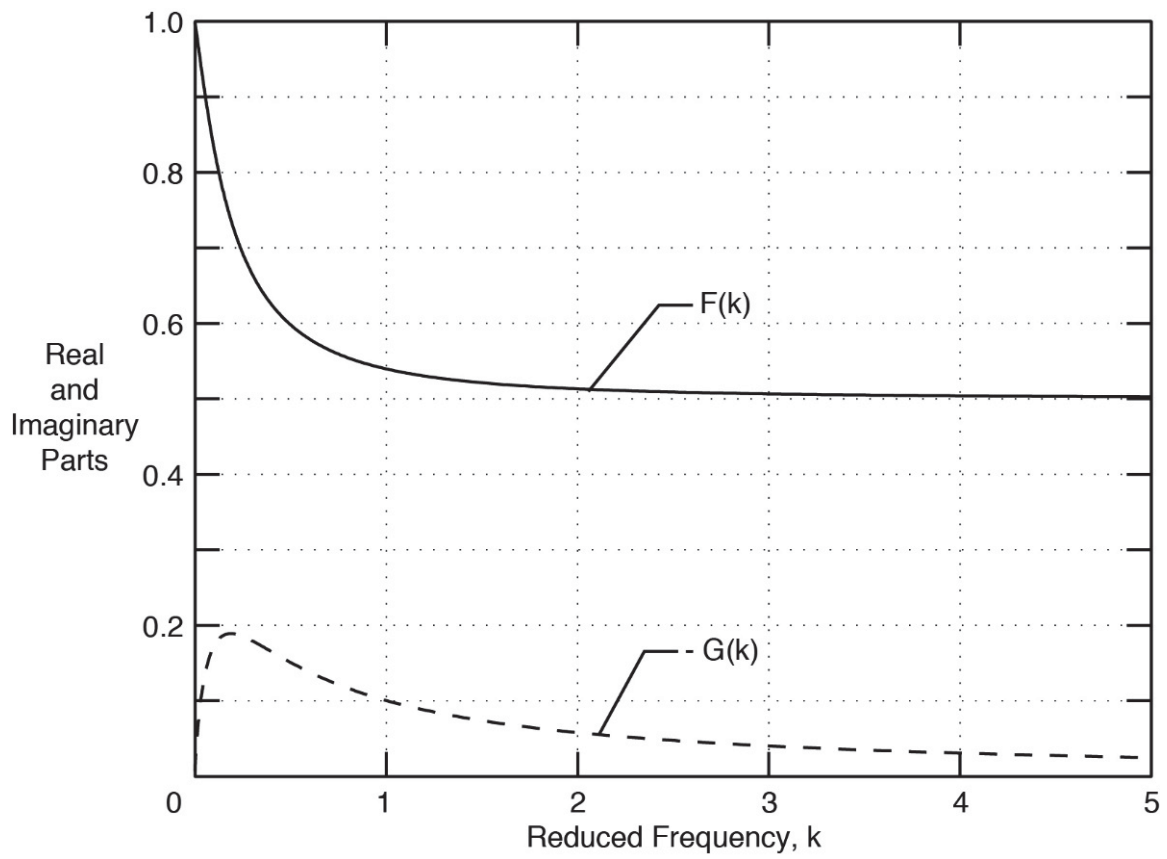
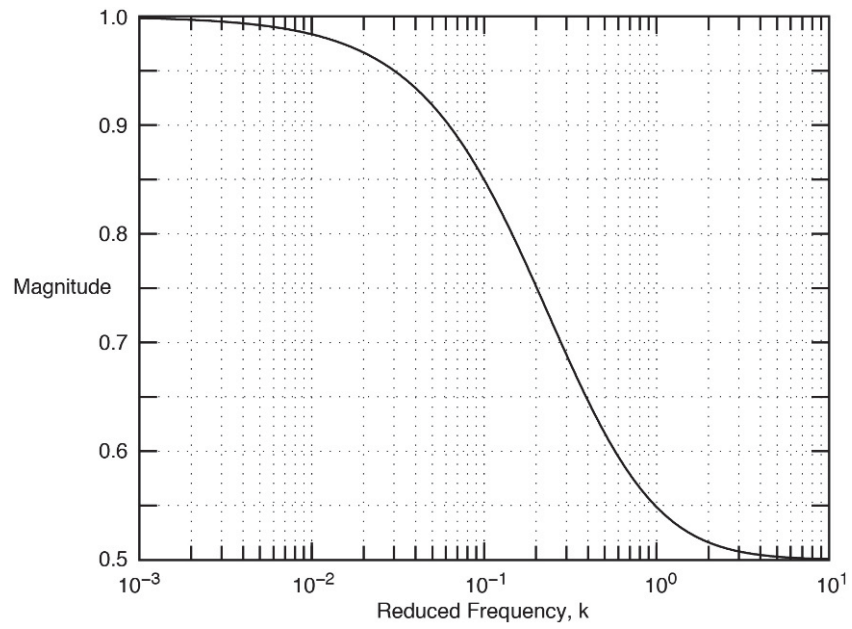
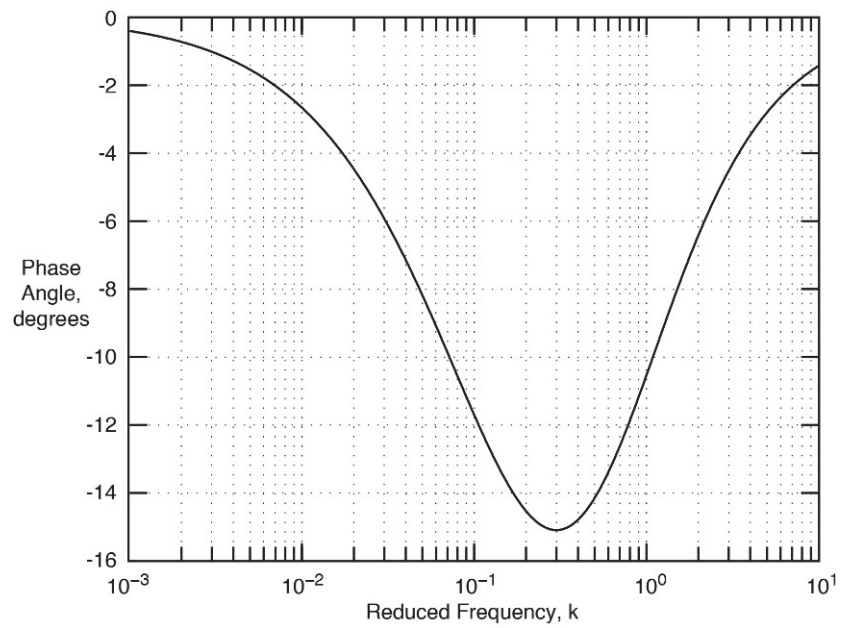


Figure A1. – Real and imaginary parts of Theodorsen's circulation function.



(a) Magnitude



(b) Phase

Figure A2. – Magnitude and phase representations of Theodorsen's circulation function.

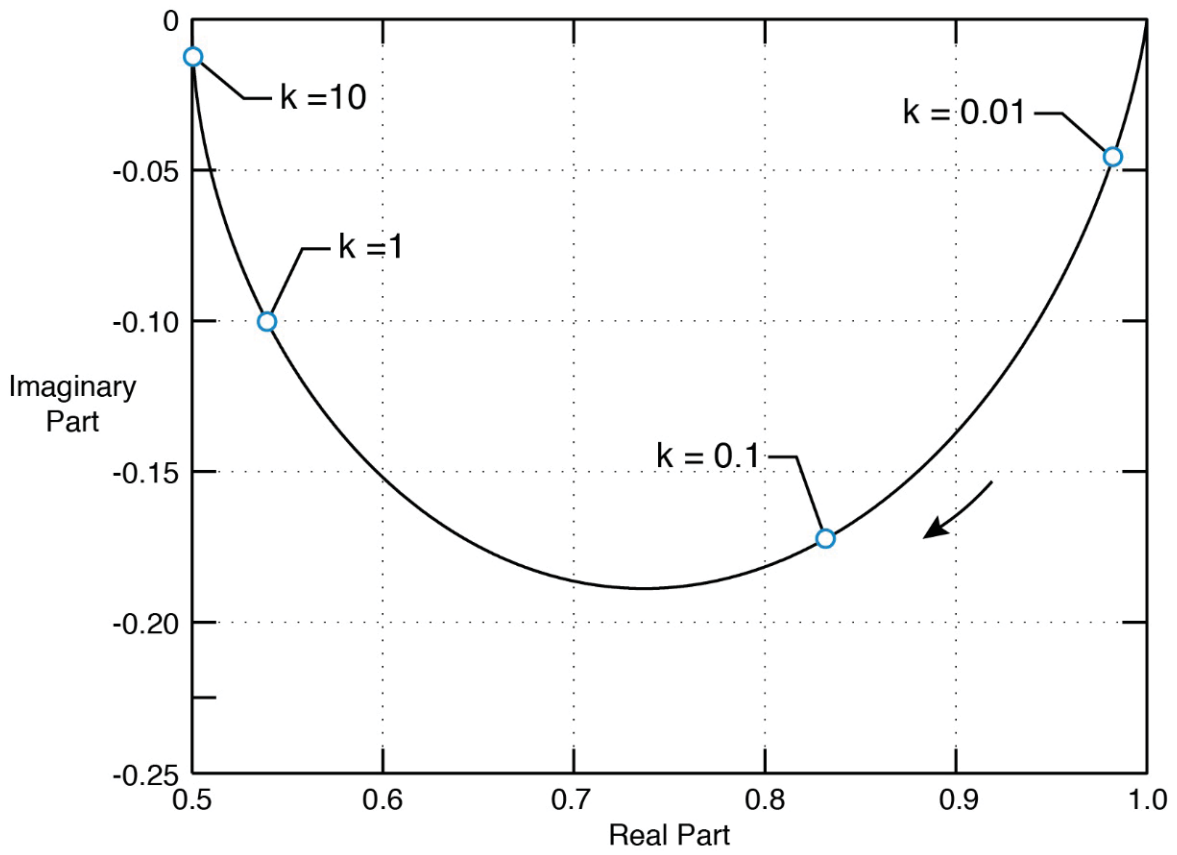


Figure A3. – Complex plane representation of Theodorsen's circulation function. Arrow indicates direction of increasing reduced frequency.

**REPORT DOCUMENTATION PAGE**

Form Approved  
OMB No. 0704-0188

The public reporting burden for this collection of information is estimated to average 1 hour per response, including the time for reviewing instructions, searching existing data sources, gathering and maintaining the data needed, and completing and reviewing the collection of information. Send comments regarding this burden estimate or any other aspect of this collection of information, including suggestions for reducing the burden, to Department of Defense, Washington Headquarters Services, Directorate for Information Operations and Reports (0704-0188), 1215 Jefferson Davis Highway, Suite 1204, Arlington, VA 22202-4302. Respondents should be aware that notwithstanding any other provision of law, no person shall be subject to any penalty for failing to comply with a collection of information if it does not display a currently valid OMB control number.  
**PLEASE DO NOT RETURN YOUR FORM TO THE ABOVE ADDRESS.**

<b>1. REPORT DATE</b> (DD-MM-YYYY) 01/09/2017	<b>2. REPORT TYPE</b> Technical Memorandum	<b>3. DATES COVERED</b> (From - To)
--	---	-------------------------------------

<b>4. TITLE AND SUBTITLE</b> Comparison of Theodorsen's Unsteady Aerodynamic Forces with Doublet Lattice Generalized Aerodynamic Forces	<b>5a. CONTRACT NUMBER</b>
	<b>5b. GRANT NUMBER</b>
	<b>5c. PROGRAM ELEMENT NUMBER</b>

<b>6. AUTHOR(S)</b>  Perry, Boyd III	<b>5d. PROJECT NUMBER</b>
	<b>5e. TASK NUMBER</b>
	<b>5f. WORK UNIT NUMBER</b> 432938.11.01.07.43.40.08

<b>7. PERFORMING ORGANIZATION NAME(S) AND ADDRESS(ES)</b>  NASA Langley Research Center Hampton, Virginia 23681-2199	<b>8. PERFORMING ORGANIZATION REPORT NUMBER</b>  L-20873
---	--

<b>9. SPONSORING/MONITORING AGENCY NAME(S) AND ADDRESS(ES)</b>  National Aeronautics and Space Administration Washington, DC 20546-0001	<b>10. SPONSOR/MONITOR'S ACRONYM(S)</b> NASA
	<b>11. SPONSOR/MONITOR'S REPORT NUMBER(S)</b> NASA-TM-2017-219667

**12. DISTRIBUTION/AVAILABILITY STATEMENT**  
Unclassified  
Subject Category 02  
Availability: NASA STI Program (757) 864-9658

**13. SUPPLEMENTARY NOTES**  
  
An Errata was added to this document October 2017

**14. ABSTRACT**  
This paper identifies the unsteady aerodynamic forces and moments for a typical section contained in the NACA Report No. 496, "General Theory of Aerodynamic Instability and the Mechanism of Flutter," by Theodore Theodorsen. These quantities are named Theodorsen's aerodynamic forces (TAFs). The TAFs are compared to the generalized aerodynamic forces (GAFs) for a very high aspect ratio wing (AR = 20) at zero Mach number computed by the doublet lattice method. Agreement between TAFs and GAFs is very-good-to-excellent. The paper also reveals that simple proportionality relationships that are known to exist between the real parts of some GAFs and the imaginary parts of others also hold for the real and imaginary parts of the corresponding TAFs.

**15. SUBJECT TERMS**  
  
Theodorsen aerodynamics; Generalized aerodynamic forces; Stability derivatives

<b>16. SECURITY CLASSIFICATION OF:</b>			<b>17. LIMITATION OF ABSTRACT</b>	<b>18. NUMBER OF PAGES</b>	<b>19a. NAME OF RESPONSIBLE PERSON</b>
<b>a. REPORT</b>	<b>b. ABSTRACT</b>	<b>c. THIS PAGE</b>			STI Help Desk(email help@sti.nasa.gov)
U	U	U	UU	35	<b>19b. TELEPHONE NUMBER</b> (Include area code) (757) 864-9658